ARTICLE IN PRESS

Control Engineering Practice ∎ (∎∎∎∎) ∎∎∎–∎∎∎

Contents lists available at ScienceDirect

Control Engineering Practice

journal homepage: www.elsevier.com/locate/conengprac

Pulse-width predictive control for LTV systems with application to spacecraft rendezvous

R. Vazquez [a,*], F. Gavilan [a], E.F. Camacho [b]

[a] Departamento de Ingeniería Aeroespacial, Escuela Superior de Ingenieros, Universidad de Sevilla, Camino de los Descubrimientos s/n, 41092 Sevilla, Spain
[b] Departamento de Ingeniería de Sistemas y Automática, Escuela Superior de Ingenieros, Universidad de Sevilla, Camino de los Descubrimientos s/n, 41092 Sevilla, Spain

ARTICLE INFO

Article history:
Received 16 October 2015
Received in revised form
23 June 2016
Accepted 24 June 2016

Keywords:
Spacecraft autonomy
Space robotics
Pulse-width modulation
Trajectory planning
Optimal trajectory
Linear time-varying systems

ABSTRACT

This work presents a Model Predictive Controller (MPC) that is able to handle Linear Time-Varying (LTV) plants with Pulse-Width Modulated (PWM) control. The MPC is based on a planner that employs a Pulse-Amplitude Modulated (PAM) or impulsive approximation as a hot-start and then uses explicit linearization around successive PWM solutions for rapidly improving the solution by means of quadratic programming. As an example, the problem of rendezvous of spacecraft for eccentric target orbits is considered. The problem is modeled by the LTV Tschauner–Hempel equations, whose state transition matrix is explicit; this is exploited by the algorithm for rapid convergence. The efficacy of the method is shown in a simulation study.

© 2016 Elsevier Ltd. All rights reserved.

1. Introduction

Frequently in applications, systems (and in particular, aerospace systems) need to be controlled by using Pulse-Width Modulated (PWM) actuators, i.e., actuators whose output level is fixed and can only be turned on and off, such as spacecraft thrusters. It would be therefore desirable to use control design methods that directly take into account this type of actuation. However, most feedback design and motion planning methods ignore variable-width pulses and approximate the control inputs either by impulses (which produce instantaneous changes in some combination of the states) or Pulse-Amplitude Modulated (PAM) control. However, neither impulsive actuation nor PAM actuation captures with precision the behavior of PWM actuators, which cannot produce arbitrary control forces, but instead can only be switched on (producing a fixed amount of control) or off (producing no control). These switching times are the only signals that can be controlled. Control design with PWM actuation poses a challenge because the system becomes nonlinear in the switching times, even if the dynamics are linear.

One can find in the literature several procedures to find an equivalent PWM solution starting from a PAM solution (see for instance Bernelli-Zazzera, Mantegazza, & Nurzia, 1998; Ieko, Ochi, & Kanai, 1999; Shieh, Wang, & Sunkel, 1996). These methods allow us to, given the PAM inputs of a system, compute PWM inputs that produce a system output which optimally approximates the output of the system when driven by the PAM signals. The results are based on the so-called Principle of Equivalent Areas, which computes the PWM signal so that its integral (area covered by the signal as time advances) during a sample time is same as the integral computed with the PAM signal. However, while these procedures are quite effective in the sense that the output produced by the approximate PWM signals is very similar to the one produced by PAM signals, they assume that the plant is linear time-invariant in order to prove the optimality of the approximation.

In this paper, Model Predictive Control (MPC) is used to directly find PWM signals to control the system. MPC (see, e.g., Camacho & Bordons, 2004) is a family of methods that originated in the late seventies and has considerably developed since then. In MPC, a process model is used to predict the future plant outputs, based on past and current values and on the proposed optimal future control actions. These actions are calculated by an optimizer taking into account a cost function as well as constraints. Since the plant is nonlinear in the control signals (ON–OFF times), the underlying optimization problem is nonlinear and possibly non-convex. To solve the problem, the algorithm starts from an initial guess computed by solving an optimal linear program with PAM or impulsive actuation, approximate the solution with ON–OFF thrusters, and then iteratively linearize around the obtained solutions to

* Corresponding author.
E-mail addresses: rvazquez1@us.es (R. Vazquez), fgavilan@us.es (F. Gavilan), eduardo@esi.us.es (E.F. Camacho).

http://dx.doi.org/10.1016/j.conengprac.2016.06.017
0967-0661/© 2016 Elsevier Ltd. All rights reserved.

improve the PWM solution. While the idea of linearization to specifically compute optimal PWM control signals in the context of MPC is, to the best knowledge of the authors, original, it must be noted that local linearization techniques have been used for optimal trajectory problems in other contexts (see e.g. Kim, Shim, & Sastry, 2002) and are standard to solve general optimization problems (a popular linearization-based method is the Sequential Quadratic Programming technique, see, e.g. Nocedal & Wright, 2006, p. 529).

As an application, the problem of rendezvous of spacecraft is considered, i.e., the controlled close encounter of two space vehicles. Autonomous spacecraft rendezvous capabilities are becoming a necessity as access to space continues increasing. The field has become very active in recent years, with a rapidly growing literature. Among others, approaches based on trajectory planning and optimization (such as Arzelier, Louembet, Rondepierre, & Kara-Zaitri, 2011, 2013; Breger & How, 2008; D'Amico et al., 2013; Deaconu, Louembet, & Théron, 2014, 2015; Gaias, D'Amico, & Ardaens, 2014; Louembet, Arzelier, & Deaconu, 2015) and predictive control, (see for instance Asawa, Nagashio, & Kida, 2006; Gavilan, Vazquez, & Camacho, 2009, 2012; Hartley, Trodden, Richards, & Maciejowski, 2012; Jewison, Erwin, & Saenz-Otero, 2015; Larsson, Berge, Bodin, & Jönsson, 2006; Leomanni, Rogers, & Gabriel, 2014; Richards & How, 2003; Rossi & Lovera, 2002; Weiss, Kolmanovsky, Baldwin, & Erwin, 2012) are emerging.

Classically, in these approaches the problem of rendezvous is modeled by using impulsive maneuvers; one computes a sequence of impulses (possibly optimal, according to a defined metric that may take into account fuel consumption and state errors), usually referred to as ΔV's, to achieve rendezvous.

Recently, Vazquez, Gavilan, and Camacho (2011, 2014), introduced a trajectory planning algorithm for spacecraft rendezvous that was able to incorporate PWM control signals. The former considered the linear time-invariant Clohessy–Wiltshire model (target orbiting in a *circular* Keplerian orbit, see Clohessy & Wiltshire, 1960). The latter extended the approach to *elliptical* target orbits by using the linear time-varying Tschauner–Hempel model (see Tschauner & Hempel, 1965). Both methods start from an initial guess computed by solving an optimal linear program with PAM or impulsive actuation, approximate the solution with ON–OFF thrusters, and then iteratively linearize around the obtained solutions to improve the PWM solution. For both circular and elliptical target orbits the algorithms are simple and reasonably fast, and simulations favorably compare with an impulsive-only approach. These results were extended in Vazquez, Gavilan, and Camacho (2015) to a decreasing-horizon model predictive controller able to take into account orbital perturbations, disturbances or model errors.

In this paper, a *receding*-horizon model predictive controller with PWM inputs is formulated for general Linear Time-Varying (LTV) plants and both alternatives (PAM or impulsive starting guess) are discussed in detail, with an application to rendezvous given at the end of the paper. The advantage of a receding-horizon formulation is that it allows a softer formulation of constraints, avoiding the need for e.g. a fixed rendezvous time, thus improving feasibility, and in addition it can be run indefinitely, allowing us to consider properties such as stability that cannot even be properly defined for decreasing-horizon algorithms.

It must be noted that, while this paper gives a very detailed application to the problem of rendezvous of spacecraft, there are many other potential applications for the methodology developed in this paper, both in the aerospace domain and in other fields, such as current control in electrical servo-motors for moving control surfaces or stabilization of coupled thermoelastic vibrations in space structures, see e.g. Bernelli-Zazzera et al. (1998).

The structure of the paper is as follows. In Section 2 the plant model is introduced. Three types of inputs are considered: PWM, PAM and impulsive. Section 3 follows with a formulation of the underlying optimization problem. Section 4 describes a method that solves the planning problem using PWM signals. Section 5 develops the model predictive controller. Next, Section 6 describes the application to spacecraft rendezvous. Section 7 presents a simulation study of the method applied to spacecraft rendezvous. The paper finishes with some remarks in Section 8.

2. System model

Consider a linear time-varying system given as

$$\dot{x} = A(t)x + B(t)u, \tag{1}$$

where $x \in \mathbb{R}^n$ is the state, $u \in \mathbb{R}^m$ is the input (control) vector, and $A(t)$ and $B(t)$ are, respectively, $n \times n$ and $n \times m$ matrices depending on time $t \geq 0$.

Considering that, for some time $t_k \geq 0$, initial conditions $x(t_k) \in \mathbb{R}^n$ are given and the input is known, the solution to (1) for $t > t_k$ is given by

$$x(t) = \Phi(t, t_k)x(t_k) + \int_{t_k}^{t} \Phi(t, s)B(s)u(s)\, ds, \tag{2}$$

where $\Phi(t, t_k)$ is the *system transition matrix*, see for instance Rugh (1996). This matrix can be computed numerically (or analytically if possible) as the unique solution to the linear matrix differential equation

$$\dot{\Phi}(t, t_k) = A(t)\Phi(t, t_k), \quad t > t_k \tag{3}$$

$$\Phi(t_k, t_k) = \mathrm{I}. \tag{4}$$

To obtain a unified notation in terms of the inputs, denote by $B_i(t)$ the i-th column of $B(t)$, corresponding to the i-th input $u_i(t)$, for $i = 1, \ldots, m$. In this paper, time intervals starting at some initial time t_k and ending at $t_{k+1} = t_k + T$ are considered, where T will be an adequate sample time. Then Eq. (2) can be written as

$$x(t_{k+1}) = \Phi(t_{k+1}, t_k)x(t_k) + \sum_{i=1}^{m} \int_{t_k}^{t_{k+1}} \Phi(t_{k+1}, s)B_i(s)u_i(s)\, ds, \tag{5}$$

The objective is solving the problem with PWM inputs. In addition, two other types of inputs are considered; they will be used as an intermediate step towards computing PWM inputs by the algorithm. All types of input are analyzed in the following sections.

2.1. Pulse width-modulated (PWM) control

In the PWM case, for each sampling interval, each input u_i is a pulse starting at time $\tau_{k,i}$ with pulse width $\kappa_{k,i}$, with constant magnitude $u_{max} = u_{k,i}^{W}$, as shown in Fig. 1 (notice that the subscript

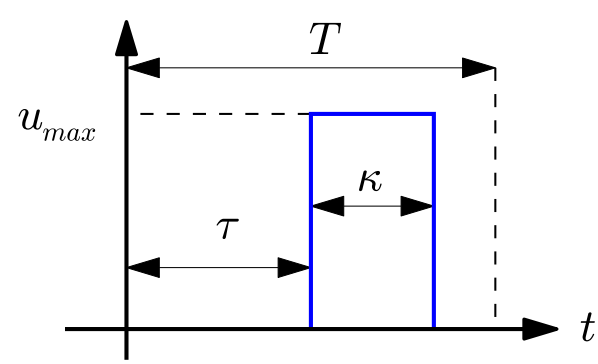

Fig. 1. PWM variables.

k is used to denote the sampling interval of each term), i.e.,

$$u_i(t) = \begin{cases} 0, & t \in [t_k, t_k + \tau_{k,i}), \\ u^W_{k,i}, & t \in [t_k + \tau_{k,i}, t_k + \tau_{k,i} + \kappa_{k,i}), \\ 0, & t \in [t_k + \tau_{k,i} + \kappa_{k,i}, t_{k+1}], \end{cases} \tag{6}$$

with $\kappa_{k,i} > 0$, $\tau_{k,i} > 0$ and $\tau_{k,i} + \kappa_{k,i} < T$, where the last constraint prevents the PWM signal from spilling over to the next time interval. Then, substituting $u_i(t)$ in (5) one obtains

$$x(t_{k+1}) = \Phi(t_{k+1}, t_k)x(t_k) + \sum_{i=1}^{m} \left(\int_{t_k+\tau_{k,i}}^{t_k+\tau_{k,i}+\kappa_{k,i}} \Phi(t_{k+1}, s)B_i(s)\, \mathrm{d}s \right) u^W_{k,i}, \tag{7}$$

and denoting

$$B^W_{k,i}(\tau_{k,i}, \kappa_{k,i}) = \int_{t_k+\tau_{k,i}}^{t_k+\tau_{k,i}+\kappa_{k,i}} \Phi(t_{k+1}, s)B_i(s)\, \mathrm{d}s, \tag{8}$$

one can write the solution as

$$x(t_{k+1}) = \Phi(t_{k+1}, t_k)x(t_k) + \sum_{i=1}^{m} B^W_{k,i}(\tau_{k,i}, \kappa_{k,i})u^W_{k,i}. \tag{9}$$

There is an important difference between a PWM input and the PAM or impulsive inputs that will be subsequently introduced. While the latter can in principle take positive or negative values at different times, the former is fixed either as positive or negative for all time. Thus, typically a PWM model has twice the number of inputs than a PAM/impulsive model. To make this explicit in the model (9), denote with a plus or minus super-index the positive or negative inputs, as follows:

$$x(t_{k+1}) = \Phi(t_{k+1}, t_k)x(t_k) + \sum_{i=1}^{m} \left[B^W_{k,i}(\tau^+_{k,i}, \kappa^+_{k,i})u^{W+}_{k,i} - B^W_{k,i}(\tau^-_{k,i}, \kappa^-_{k,i})u^{W-}_{k,i} \right], \tag{10}$$

with $u^{W+}_{k,i}$, $\tau^+_{k,i}$, $\kappa^+_{k,i}$ and $u^{W-}_{k,i}$, $\tau^-_{k,i}$, $\kappa^-_{k,i}$ denoting, respectively, the magnitude, start, and width of the positive and negative i-th input pulses.

2.2. Pulse amplitude-modulated (PAM) control

In this case, each control $u_i(t)$ in (5) is constant inside the interval $[t_k, t_{k+1})$, and equal to $u^A_{k,i}$. Then, substituting $u_i(t)$ in (5) one obtains

$$x(t_{k+1}) = \Phi(t_{k+1}, t_k)x(t_k) + \sum_{i=1}^{m} \left(\int_{t_k}^{t_{k+1}} \Phi(t_{k+1}, s)B_i(s)\, \mathrm{d}s \right) u^A_{k,i}, \tag{11}$$

and denoting by

$$B^A_{k,i} = \int_{t_k}^{t_{k+1}} \Phi(t_{k+1}, s)B_i(s)\, \mathrm{d}s, \tag{12}$$

the solution can be written as

$$x(t_{k+1}) = \Phi(t_{k+1}, t_k)x(t_k) + \sum_{i=1}^{m} B^A_{k,i}u^A_{k,i}. \tag{13}$$

2.3. Impulsive control

In this case, $u_i(t) = u^I_{k,i}\delta(t - (t_k + \tau_{k,i}))$, where $\delta(t)$ is Dirac's delta function, $t_k + \tau_{k,i}$ is the instant at which the impulse is given, and $u_{k,i}$ is the magnitude of the impulse. Then, assuming $0 < \tau_{k,i} < T$ for all i (all the impulses are given inside the considered time interval) and substituting $u_i(t)$ in (5) one obtains

$$x(t_{k+1}) = \Phi(t_{k+1}, t_k)x(t_k) + \sum_{i=1}^{m} \Phi(t_{k+1}, t_k + \tau_i)B_i(t_k + \tau_i)u^I_{k,i}, \tag{14}$$

and denoting by $B^I_{k,i}(\tau_{k,i}) = \Phi(t_{k+1}, \tau_i)B_i(t_k + \tau_i)$,

$$x(t_{k+1}) = \Phi(t_{k+1}, t_k)x(t_k) + \sum_{i=1}^{m} B^I_{k,i}(\tau_{k,i})u^I_{k,i}. \tag{15}$$

2.4. Discretization and compact notation

Consider now a sequence of time instants $t_k = t_0 + kT$, $k = 0, \ldots$, and denote $x_k = x(t_k)$. Then, it is possible to write, for both PAM and impulsive control,

$$x_{k+1} = A_k x_k + B_k U_k, \tag{16}$$

where $A_k = \Phi(t_{k+1}, t_k)$, and B_k and U_k depend on the input type. Note that, in general, A_k and B_k are matrices that must be computed numerically. In the PWM case, write

$$x_{k+1} = A_k x_k + B^+_k U^+_k - B^-_k U^-_k, \tag{17}$$

where B^+_k is a matrix whose i-th column is $B^W_{k,i}(\tau^+_{k,i}, \kappa^+_{k,i})$ and U^+_k, τ^+_k, and κ^+_k are column vectors whose i-th entries are, respectively, $u^W_{k,i}$, $\tau^+_{k,i}$ and $\kappa^+_{k,i}$. The same definitions (with minus super-index) are used for the negative pulses. Then, to reach model (16), define

$$B_k = \begin{bmatrix} B^+_k & -B^-_k \end{bmatrix}, \quad U_k = \begin{bmatrix} U^+_k \\ U^-_k \end{bmatrix},$$
$$\tau_k = \begin{bmatrix} \tau^+_k \\ \tau^-_k \end{bmatrix}, \quad \kappa_k = \begin{bmatrix} \kappa^+_k \\ \kappa^-_k \end{bmatrix}. \tag{18}$$

The definitions of B_k are simpler for the other types of actuation. In the PAM case, B_k is a matrix whose i-th column is $B^A_{k,i}$ and U_k a column vector whose i-th entry is $u^A_{k,i}$. In the impulsive case, B_k is a matrix whose i-th column is $B^I_{k,i}(\tau_{k,i})$, and U_k and τ_k are column vectors whose i-th entries are, respectively, $u^I_{k,i}$ and $\tau_{k,i}$.

Next a compact formulation is developed to simplify the notation of the problem. The state at time t_{k+j+1}, given the state x_k at time t_k, and the input signals from t_k to time t_{k+j}, is computed by applying recursively, in the PAM and impulsive cases, Eq. (16). One obtains

$$x_{k+j+1} = A_{k+j+1,k}x_k + \sum_{i=k}^{k+j} A_{k+j,i}B_{k,i}U_{k,i}, \tag{19}$$

where the definition $A_{k,k} = \mathrm{I}$, $A_{k+1,k} = A_k$, and if $j > 0$ then $A_{k+j+1,k} = A_{k+j}A_{k+j-1}\ldots A_k$ has been used. Define now $\mathcal{X}_k$ and $\mathcal{U}_k$ as a *stack vector* of N_p state and input vectors, respectively, spanning from time t_{k+1} to time t_{k+N_p} for the state and from time t_k to time t_{k+N_p-1} for the controls, where N_p is the planning horizon:

$$\mathcal{X}_k = \begin{bmatrix} x_{k+1} \\ \vdots \\ x_{k+N_p} \end{bmatrix}, \quad \mathcal{U}_k = \begin{bmatrix} U_k \\ \vdots \\ U_{k+N_p-1} \end{bmatrix}.$$

Similarly, for the impulsive and PWM cases, define

$$\Gamma_k = \begin{bmatrix} \tau_k \\ \vdots \\ \tau_{k+N_p-1} \end{bmatrix}, \quad \Lambda_k = \begin{bmatrix} \kappa_k \\ \vdots \\ \kappa_{k+N_p-1} \end{bmatrix}, \quad \Upsilon_k = \begin{bmatrix} \Gamma_k \\ \Lambda_k \end{bmatrix}$$

Then one can write

$$\mathcal{X}_k = F_k x_k + G_k \mathcal{U}_k, \tag{20}$$

where G_k is a block lower triangular matrix of size $nN_p \times mN_p$, defined as

$$G_k = \begin{bmatrix} B_k & 0 & \cdots & 0 \\ A_{k+2,k+1}B_k & B_{k+1} & \cdots & 0 \\ \vdots & \vdots & \ddots & \vdots \\ A_{k+N_p,k+1}B_k & A_{k+N_p,k+2}B_{k+1} & \cdots & B_{k+Np-1} \end{bmatrix}, \tag{21}$$

this is, its non-null blocks are defined by $(G_k)_{jl} = A_{k+j,k+l}B_{k+l-1}$, and the matrix F_k is defined as:

$$F_k = \begin{bmatrix} A_{k+1,k} \\ A_{k+2,k} \\ \vdots \\ A_{k+N_p,k} \end{bmatrix}. \tag{22}$$

Note that, in the impulsive case, G_k is a (nonlinear) function of Γ_k, whereas in the PWM case it is a (nonlinear) function of Υ_k. To avoid lengthy expressions this dependence has been omitted. In the PWM case, $\mathcal{U}_k$ is fixed whereas in the other cases it is the input variable.

3. Formulation of the planning problem

Next the planning problem is formulated, introducing the constraints and the objective function. The formulation is done for the three types of control signals.

3.1. Constraints on the problem

First constraints on the state and input are introduced. While only inequalities are considered, equality constraints would be treated similarly.

3.1.1. Inequality constraints on the state

The state can be subject to inequality constraints along the planning horizon, which can vary as time advances. These can be formulated in general as $C_{S,k}\mathcal{X}_k \le d_{S,k}$, and using (20), one reaches a expression in terms of inputs, namely

$$C_{S,k}G_k\mathcal{U}_k \le d_{S,k} - C_{S,k}F_kx_k. \tag{23}$$

3.1.2. Input constraints

Input constraints are different depending on the type of input.

In the PWM case, the inputs $\mathcal{U}_k$ are fixed, but the start time of impulse, $t_k + \tau_k$, and its end, $t_k + \tau_k + \kappa_k$, must be within the time interval both for negative and positive pulses. Thus

$$0 \le \Gamma_k, \tag{24}$$

$$0 \le \Lambda_k, \tag{25}$$

$$\Gamma_k + \Lambda_k \le \mathcal{T}, \tag{26}$$

with $\mathcal{T}$ being a stack vector of the same size than Γ_k and Λ_k, containing the sampling time T in each component. These inequalities can be summarized as

$$C_W\Upsilon_k \le d_W. \tag{27}$$

In the PAM case, the inputs are limited above and below. Thus

$$\underline{U}_{PAM} \le \mathcal{U}_k \le \overline{U}_{PAM}, \tag{28}$$

where $\underline{U}_{PAM}$ and $\underline{U}_{PAM}$ are stacked vectors containing the lower and upper bounds of the control forces exerted by each thruster at each sampling time.

In the impulsive case, the inputs u_k are limited above and below, but also the times of impulse, $t_k + \tau_k$, must be within the time interval. Thus

$$\underline{U}_{IMP} \le \mathcal{U}_k \le \overline{U}_{IMP}, \tag{29}$$

$$0 \le \Gamma_k \le \mathcal{T}, \tag{30}$$

where, again $\underline{U}_{IMP}$ and $\underline{U}_{IMP}$ are stacked vectors containing the lower and upper bounds of the impulses exerted by each thruster at each sampling time.

3.2. Objective function

At each sampling time k, the objective function to be minimized is a combination of the 1-norm of the control signal, which is denoted as $J_{\mathcal{U},k}$, (which gives an estimation of fuel consumption in case the control signal is thrust, see Section 6) and a weighted squared 2-norm of the state, which is denoted as $J_{\mathcal{X},k}$, both taken over the planning horizon. Thus,

$$J_k = J_{\mathcal{U},k} + \alpha J_{\mathcal{X},k}, \tag{31}$$

where α is a positive constant that allows us to give a relative weight between input cost and state error. Note that α could be included inside any two of the state or control cost indexes; however it is convenient to have a single parameter controlling the relative weight between the two. $J_{\mathcal{X},k}$ is computed as

$$J_{\mathcal{X},k} = \mathcal{X}_k^TQ_k\mathcal{X}_k, \tag{32}$$

for $Q_k > 0$. Written in terms of the inputs and the starting point x_k, an equivalent objective function reads

$$J'_{\mathcal{X},k} = 2x_k^TF_k^TQ_kG_k\mathcal{U}_k + \mathcal{U}_k^TG_k^TQ_kG_k\mathcal{U}_k, \tag{33}$$

an expression in which the constant term $x_k^TF_k^TQ_kF_kx_k$—which does not play a role in the planning optimization as it is constant, given x_k—is neglected (notice the prime in $J'_{\mathcal{X},k}$ introduced to reflect this change).

The value of $J_{\mathcal{U},k}$ does, however, depend on the control type. Its definition is shown in the next sections according to the type of control input.

3.2.1. PWM control inputs

For the case of PWM control inputs, using definition (6) it can be seen that the objective function $J_{\mathcal{U},k}$ is given by

$$J_{\mathcal{U},k} = \sum_{j=k}^{k+N_p-1}\left[(U_j^+)^T\kappa_j^+ + (U_j^-)^T\kappa_j^-\right] = \mathcal{U}_k^T\Lambda_k = \mathcal{H}_k^J\Upsilon_k, \tag{34}$$

with $\mathcal{H}_k^J$ defined by blocks as

$$\mathcal{H}_k^J = \begin{bmatrix} 0 & \mathcal{U}_k^T \end{bmatrix}. \tag{35}$$

The times Γ_k where inputs start does not play a role in the cost function (only their duration Λ_k).

3.2.2. PAM control inputs

For the case of PAM control inputs, it can be seen that the objective function $J_U(k)$ is given by

$$J_{\mathcal{U},k} = \sum_{j=k}^{k+N_p-1} T \parallel U_j \parallel_1 = T \parallel \mathcal{U}_k \parallel_1. \tag{36}$$

3.2.3. Impulsive control inputs

For the case of impulsive control inputs, $J_{\mathcal{U},k}$ is given by

$$J_{\mathcal{U},k} = \sum_{j=k}^{k+N_p-1} \| U_j \|_1 = \| \mathcal{U}_k \|_1, \tag{37}$$

where it should be noticed that, as in the PWM case, the location $\tau_{k,i}$ of the impulses does not play a role in the cost function.

3.3. Planning optimization problem

Now, for each of the input types, one can formulate a planning optimization problem starting from initial condition x_k at time t_k, with a planning horizon of N_p, as follows.

3.3.1. PWM control inputs

For PWM control inputs, the planning optimization problem is formulated as

$$\begin{aligned} \min_{\Upsilon_k} \quad & 2x_k^T F_k^T Q_k G_k(\Upsilon_k)\mathcal{U}_k + \mathcal{U}_k^T G_k^T(\Upsilon_k) Q_k G_k(\Upsilon_k)\mathcal{U}_k + \alpha \mathcal{H}_k^l \Upsilon_k, \\ \text{s. t.} \quad & C_{S,k} G_k(\Upsilon_k)\mathcal{U}_k \le d_{S,k} - C_{S,k} F_k x_k, \\ & C_W \Upsilon_k \le d_W. \end{aligned} \tag{38}$$

Notice that $\mathcal{U}_k$ is known, and one has to compute the start and width of the pulses, contained in Υ_k (start and duration of pulses), which enter nonlinearly in the optimization problem. The dependence of G_k on Υ_k has been made explicit, because it is the variable with respect to which the optimization is carried out.

3.3.2. PAM control inputs

For PAM control inputs, the planning optimization problem is formulated as

$$\begin{aligned} \min_{\mathcal{U}_k} \quad & 2x_k^T F_k^T Q_k G_k \mathcal{U}_k + \mathcal{U}_k^T G_k^T Q_k G_k \mathcal{U}_k + \alpha T \| \mathcal{U}_k \|_1, \\ \text{s.t.} \quad & C_{S,k} G_k \mathcal{U}_k \le d_{S,k} - C_{S,k} F_k x_k, \\ & \underline{U}_{PAM} \le \mathcal{U}_k \le \overline{U}_{PAM}. \end{aligned} \tag{39}$$

3.3.3. Impulsive control inputs

For impulsive control inputs, the planning optimization problem is formulated as

$$\begin{aligned} \min_{\mathcal{U}_k, \Gamma_k} \quad & 2x_k^T F_k^T Q_k G_k(\Gamma_k)\mathcal{U}_k + \mathcal{U}_k^T G_k^T(\Gamma_k) Q_k G_k(\Gamma_k)\mathcal{U}_k + \alpha \| \mathcal{U}_k \|_1, \\ \text{s. t.} \quad & C_{S,k} G_k(\Gamma_k)\mathcal{U}_k \le d_{S,k} - C_{S,k} F_k x_k, \\ & \underline{U}_{IMP} \le \mathcal{U}_k \le \overline{U}_{IMP}, \\ & 0 \le \Gamma_k \le \mathcal{T}. \end{aligned} \tag{40}$$

The dependence of G_k on Γ_k (location of impulses) has been made explicit to emphasize that the optimization problem is nonlinear.

4. PWM planning algorithm

In this section the subindex k is kept even though it does not play any role. For a "pure" planning problem, it could be set to zero. However, k will be useful when defining the MPC algorithm in Section 5.

Consider now the problem (38), given x_k and $\mathcal{U}_k$. The planning algorithm proposed in this paper follows the next steps (which will be further explained in the next sections).

Step 1 (Section 4.1): Solve either the PAM optimization problem (39), or the impulsive problem (40) with a fixed Γ_k, to provide an initial guess of the PWM solution.

Step 2 (Section 4.2): The PAM or impulsive control inputs resulting from the optimization algorithm in Step 1 are converted to a sequence of PWM inputs. Denote this initial sequence by ${\Upsilon_k}^0$. Set i=0.

Step 3 (Section 4.3): The trajectory of the system with the PWM inputs ${\Upsilon_k}^i$ is computed analytically (if possible) or numerically by using Eq. (20). Denote the trajectory by $\mathcal{X}_k^i$.

Step 4 (Section 4.4): The system with PWM inputs is *linearized* around $\mathcal{X}_k^i$, thus obtaining a linear, explicit plant with respect to *increments*, denoted as ${\Delta_k}^i$, in the PWM inputs. Then a quadratic program can be posed and solved to find the increments that improve the cost function.

Step 5 (Section 4.4): The resulting solution ${\Delta_k}^i$ is used to improve the approximation towards the real solution, by setting $\Upsilon_k^{i+1} = \Upsilon_k^i + \Delta_k^i$. Increase i by one and go back to Step 3. The process is iterated until the solution converges or time is up. Note that if there is no convergence, or if Step 4 cannot be performed (there is no solution), the initial sequence ${\Upsilon_k}^0$ can be used as a backup.

Note that an alternative solution would be to use a "generic" SQP algorithm (see, e.g. Nocedal & Wright, 2006, p. 529), or using a dedicated MPC Toolkit like ACADO (described in Houska, Ferreau, & Diehl, 2011). There are several key features that differentiate these generic approaches from the tailored procedure presented here. First, the problem formulation itself (in the continuous-time domain) is used in the linearization (Step 4). This allows us to explicitly find the derivatives in terms of PWM inputs. The hot-start approach (Step 1), based on impulsive or PAM signals, is also an important feature of the algorithm. Finally, for specific applications (see e.g. Section 6), this procedure can easily use explicit closed-form solutions of the system dynamics. This might be advantageous for applications with less computational resources. In any case, other methods that could be tailored to use these elements would obviously benefit from them.

In the following sections, all the steps in the algorithm are described.

4.1. Step 1: Computation of PAM/impulsive control input

First, one has to choose whether to find an initial guess using a PAM approach or an impulsive approach. The PAM guess is more suitable if one expects wide pulses, whereas the impulsive guess is best when the pulses are rather short.

If a PAM guess is chosen, it is computed from (39), setting $\overline{U}_{PAM} = T\mathcal{U}_k^+$ and $\underline{U}_{PAM} = T\mathcal{U}_k^-$. The maximum and minimum is set in this way, so that the solution can always be converted to PWM following the procedure of Section 4.2. On the other hand, the impulsive guess is computed from (40), setting $\overline{U}_{IMP} = \mathcal{U}_k^+$ and $\underline{U}_{IMP} = \mathcal{U}_k^-$. The impulsive guess also requires to set the impulse location Γ_k to some pre-determined value, so only the impulse magnitude (which appears linearly in (40)) is unknown. Typical positions would be the middle of the interval (all entries of Γ_k equal to $T/2$) or start of the interval ($\Gamma_k = 0$).

4.2. Step 2: Initial PWM solution: adapting the PAM/impulsive solution

The PAM/impulsive solution from Section 4.1, $\mathcal{U}$, is transformed to a PWM sequence of inputs, as follows:

1. From $\mathcal{U}$ extract $u_{j,i}^A$ (or $u_{j,i}^I$ if the initial solution is of impulsive type) for $j = k, \ldots, k + N_p - 1$ and $i = 1, \ldots, m$. Also extract $\tau_{j,i}$ if the initial solution is of impulsive type.
2. If the initial solution is of PAM type, set

$$\tau_{j,i}^+(t) = \begin{cases} \dfrac{Tu_{j,i}^A}{u_{j,i}^{W\pm}}, & u_{j,i}^A > 0, \\ 0, & u_{j,i}^A \le 0, \end{cases} \qquad \tau_{j,i}^-(t) = \begin{cases} -\dfrac{Tu_{j,i}^A}{u_{j,i}^{W\pm}}, & u_{j,i}^A < 0, \\ 0, & u_{j,i}^A \ge 0, \end{cases} \tag{41}$$

and if the initial solution is of impulsive type,

$$\tau_{j,i}^{+} = \begin{cases} \dfrac{u_{j,i}^{I}}{u_{j,i}^{W\pm}}, & u_{j,i}^{A} > 0, \\ 0, & u_{j,i}^{I} \le 0, \end{cases} \qquad \tau_{j,i}^{-} = \begin{cases} -\dfrac{u_{j,i}^{I}}{u_{j,i}^{W\pm}}, & u_{j,i}^{A} < 0, \\ 0, & u_{j,i}^{I} \ge 0. \end{cases} \tag{42}$$

3. In the PAM case, the PWM input should be centered in the interval: $\kappa_{j,i}^{+} = \frac{T-\tau_{j,i}^{+}}{2}$, $\kappa_{j,i}^{-} = \frac{T-\tau_{j,i}^{-}}{2}$. In the impulsive case, the PWM input should be centered around the chosen $\tau_{j,i}$ (corrected if necessary to avoid spillover), i.e.

$$\kappa_{j,i}^{+} = \begin{cases} 0, & \tau_{j,i} - \dfrac{\tau_{j,i}^{+}}{2} < 0, \\ T - \tau_{j,i}^{+}, & \tau_{j,i} + \dfrac{\tau_{j,i}^{+}}{2} > T, \\ \tau_{j,i} - \dfrac{\tau_{j,i}^{+}}{2}, & \text{otherwise}, \end{cases} \tag{43}$$

$$\kappa_{j,i}^{-} = \begin{cases} 0, & \tau_{j,i} - \dfrac{\tau_{j,i}^{-}}{2} < 0, \\ T - \tau_{j,i}^{-}, & \tau_{j,i} + \dfrac{\tau_{j,i}^{-}}{2} > T, \\ \tau_{j,i} - \dfrac{\tau_{j,i}^{-}}{2}, & \text{otherwise}, \end{cases} \tag{44}$$

4. From $\tau_{j,i}^{+}$, $\tau_{j,i}^{-}$, $\kappa_{j,i}^{+}$, and $\kappa_{j,i}^{-}$, construct Γ_k and Λ_k and thus Υ_k.

The PWM signals Γ_k, Λ_k constructed by this method produce a moderately similar (but not equal) output to the system driven by PAM or impulsive signals, but as time advances the output might considerably differ. See Shieh et al. (1996), Ieko et al. (1999) and Bernelli-Zazzera et al. (1998) for more details and other methods. In addition, these approximated PWM controls are not optimal (with respect to the real system with PWM inputs), and they might not even satisfy the constraints. However, this solution is only used as an initialization for the optimization algorithm proposed next. Denote as Υ_k^{0} the found solution and set $i=0$.

4.3. Step 3: Computation of trajectories under PWM inputs

For the current iteration i, apply (20) to compute the states of the system $\mathcal{X}_k^{i}$ at all times, with PWM inputs Υ_k^{i}. The matrix G_k might need to be computed numerically if an explicit solution for the integrals (8) is not known.

4.4. Steps 4 and 5: Refined PWM solution: an optimization algorithm

To linearize (20) around inputs Υ_k^{i}, notice from (8) that

$$\begin{aligned} \frac{\partial}{\partial \tau_{k,i}} B_{k,i}^{W}\Big(\tau_{k,i}, \kappa_{k,i}\Big) &= \frac{\partial}{\partial \tau_{k,i}} \int_{t_k+\tau_{k,i}}^{t_k+\tau_{k,i}+\kappa_{k,i}} \Phi\Big(t_{k+1}, s\Big) B_i\Big(s\Big)\, \mathrm{d}s, \\ &= \Phi\Big(t_{k+1}, t_k + \tau_{k,i} + \kappa_i\Big) B_i\Big(t_k + \tau_{k,i} + \kappa_{k,i}\Big) \\ &\quad - \Phi\Big(t_{k+1}, t_k + \tau_{k,i}\Big) B_i\Big(t_k + \tau_{k,i}\Big), \end{aligned} \tag{45}$$

and

$$\begin{aligned} \frac{\partial}{\partial \kappa_{k,i}} B_{k,i}^{W}\Big(\tau_{k,i}, \kappa_{k,i}\Big) &= \frac{\partial}{\partial \kappa_{k,i}} \int_{t_k+\tau_{k,i}}^{t_k+\tau_{k,i}+\kappa_{k,i}} \Phi\Big(t_{k+1}, s\Big) B_i\Big(s\Big)\, \mathrm{d}s, \\ &= \Phi\Big(t_{k+1}, t_k + \tau_{k,i} + \kappa_i\Big) B_i\Big(t_k + \tau_{k,i} + \kappa_{k,i}\Big). \end{aligned} \tag{46}$$

Thus, (16) can be explicitly linearized around some given $\bar{\tau}_k^{+}$, $\bar{\tau}_k^{-}$ and $\bar{\kappa}_k^{+}$, $\bar{\kappa}_k^{-}$, reaching

$$x_{k+1} = A_k x_k + B_k U_k + B_k^{\Delta\tau} \delta\tau_k + B_k^{\Delta\kappa} \delta\kappa_k, \tag{47}$$

where B_k is computed with $\bar{\tau}_k^{+}$, $\bar{\tau}_k^{-}$, $\bar{\kappa}_k^{+}$, and $\bar{\kappa}_k^{-}$ (notice that the two first terms of the right-hand-side part correspond to the nominal terms of the Taylor series expansion), and define

$$B_k^{\Delta\tau} = \begin{bmatrix} B_k^{\delta\tau^{+}} & B_k^{\delta\tau^{-}} \end{bmatrix}, \quad B_k^{\Delta\kappa} = \begin{bmatrix} B_k^{\delta\kappa^{+}} & B_k^{\delta\kappa^{+}} \end{bmatrix}, \tag{48}$$

$$\delta\tau_k = \begin{bmatrix} \bar{\tau}_k^{+} - \tau_k^{+} \\ \bar{\tau}_k^{-} - \tau_k^{-} \end{bmatrix}, \quad \delta\kappa_k = \begin{bmatrix} \bar{\kappa}_k^{+} - \kappa_k^{+} \\ \bar{\kappa}_k^{-} - \kappa_k^{-} \end{bmatrix}, \tag{49}$$

where the i-th entries of the B_k^{δ} matrices in (48) are given, respectively, by

$$\begin{aligned} (B_k^{\delta\tau^{+}})_i &= \Phi\Big(t_k + T, t_k + \bar{\tau}_{k,i}^{+} + \bar{\kappa}_{k,i}^{+}\Big) \times B_i\Big(t_k + \bar{\tau}_{k,i}^{+} + \bar{\kappa}_{k,i}^{+}\Big) u_{k,i}^{W+} \\ &\quad - \Phi\Big(t_k + T, t_k + \bar{\tau}_{k,i}^{+}\Big) B_i\Big(t_k + \bar{\tau}_{k,i}^{+}\Big) u_{k,i}^{W+} \end{aligned} \tag{50}$$

$$\begin{aligned} (B_k^{\delta\tau^{-}})_i &= -\Phi\Big(t_k + T, t_k + \bar{\tau}_{k,i}^{-} + \bar{\kappa}_{k,i}^{-}\Big) \times B_i\Big(t_k + \bar{\tau}_{k,i}^{-} + \bar{\kappa}_{k,i}^{-}\Big) u_{k,i}^{W-} \\ &\quad + \Phi\Big(t_k + T, t_k + \bar{\tau}_{k,i}^{-}\Big) B_i\Big(t_k + \bar{\tau}_{k,i}^{-}\Big) u_{k,i}^{W-} \end{aligned} \tag{51}$$

$$(B_k^{\delta\kappa^{+}})_i = \Phi(t_k + T, t_k + \bar{\tau}_{k,i}^{+} + \bar{\kappa}_{k,i}^{+}) \times B_i(t_k + \bar{\tau}_{k,i}^{+} + \bar{\kappa}_{k,i}^{+}) u_{k,i}^{W+}, \tag{52}$$

$$(B_k^{\delta\kappa^{-}})_i = -\Phi(t_k + T, t_k + \bar{\tau}_{k,i}^{-} + \bar{\kappa}_{k,i}^{-}) \times B_i(t_k + \bar{\tau}_{k,i}^{-} + \bar{\kappa}_{k,i}^{-}) u_{k,i}^{W-} \tag{53}$$

Thus, defining stack vectors with the increments in the PWM variables at step i as

$$\Delta\Gamma_k^{i} = \begin{bmatrix} \delta\tau_k \\ \vdots \\ \delta\tau_{k+N_p-1} \end{bmatrix}, \quad \Delta\Lambda_k^{i} = \begin{bmatrix} \delta\kappa_k \\ \vdots \\ \delta\kappa_{k+N_p-1} \end{bmatrix},$$

and grouping all increments as

$$\Delta_k^{i} = \begin{bmatrix} \Delta\Gamma_k^{i} \\ \Delta\Lambda_k^{i} \end{bmatrix}, \quad B_k^{\Delta} = \begin{bmatrix} B_k^{\Delta\tau} \\ B_k^{\Delta\kappa} \end{bmatrix},$$

and defining G_k^{Δ} as in (21), i.e.,

$$G_k^{\Delta} = \begin{bmatrix} B_k^{\Delta} & 0 & \cdots & 0 \\ A_{k+2,k+1} B_k^{\Delta} & B_{k+1}^{\Delta} & \cdots & 0 \\ \vdots & \vdots & \ddots & \vdots \\ A_{k+N_p,k+1} B_k^{\Delta} & A_{k+N_p,k+2} B_{k+1}^{\Delta} & \cdots & B_{k+Np-1}^{\Delta} \end{bmatrix}, \tag{54}$$

one can write

$$\mathcal{X}_k^i \approx F_k x_k + G_k(\Upsilon_k^i)\mathcal{U}_k + G_k^{\Delta}(\Upsilon_k^i)\Delta_k^i, \tag{55}$$

The state constraints (23) become

$$C_{S,k}G_k^{\Delta}(\Upsilon_k^i)\Delta_k^i \le d_{S,k} - C_{S,k}F_k x_k - G_k(\Upsilon_k^i)\mathcal{U}_k. \tag{56}$$

The constraints on $\Delta\Gamma_k^i$ and $\Delta\Lambda_k^i$ are as follows:

$$-C_W\Delta_k^i \le d_W - C_W\Upsilon_k^i, \tag{57}$$

$$-\Delta_{max} \le \Delta_k^i \le \Delta_{max}, \tag{58}$$

where the last constraint (58) is used to avoid large variations that might make the linearization approximation to fail. All these constraints are might be summarized as

$$C_{\Delta}\Delta_k^i \le d_{\Delta}. \tag{59}$$

Finally, the objective function can be rewritten in terms of $\Delta_k{}^i$ as $J_k^i = J_k^i(\Upsilon_k^i) + J_k^{\Delta}(\Upsilon_k^i, \Delta_k^i)$, where

$$J_k^i = 2x_k^T F_k^T Q_k G_k(\Upsilon_k^i)\mathcal{U}_k + \mathcal{U}_k^T G_k^T(\Upsilon_k^i) Q_k G_k(\Upsilon_k^i)\mathcal{U}_k + \alpha\mathcal{H}_k^J\Upsilon_k^i, \tag{60}$$

$$J_k^{\Delta} = 2\left(x_k^T F_k^T + \mathcal{U}_k^T G_k^T\left(\Upsilon_k^i\right)\right)Q_k G_k^{\Delta}\left(\Upsilon_k^i\right)\Delta_k^i + (\Delta_k^i)^T G_k^{\Delta T}\left(\Upsilon_k^i\right)Q_k G_k^{\Delta}\left(\Upsilon_k^i\right)\Delta_k^i + \alpha\mathcal{H}_k^J\Delta_k^i. \tag{61}$$

Noting that $J_k{}^{\Delta}$ is quadratic in $\Delta_k{}^i$, a quadratic optimization program with linear restriction, formulated on the output increments, can be posed as follows:

$$\begin{aligned} \min_{\Delta_k^i} \quad & J_k^{\Delta}(\Upsilon_k^i, \Delta_k^i) \\ \text{s. t.:} \quad & C_{S,k}G_k^{\Delta}(\Upsilon_k^i)\Delta_k^i \le d_{S,k} - C_{S,k}F_k x_k - G_k(\Upsilon_k^i)\mathcal{U}_k, \\ & C_{\Delta}\Delta_k^i \le d_{\Delta}. \end{aligned} \tag{62}$$

The solution Δ_k is used to recompute new PWM inputs, $\Upsilon_k^{i+1} = \Upsilon_k^i + \Delta_k^i$. Then the linearization process can be repeated around the new Υ_k^{i+1}, refining the solution in each iteration.

5. Model predictive control with PWM inputs

In this section, building upon the trajectory planning algorithm of Section 4, which is open-loop and has a finite time-horizon, a closed-loop algorithm is developed based on the ideas of model predictive control (also known as receding horizon control). Model predictive control closes the loop by simply re-planning the maneuver at each time step, after applying just the set of control inputs corresponding to the first time step, and keeps looking ahead N_p time steps. Thus, the algorithm starts at $k=0$ and is repeated for each k. The re-planning is done from the actual position at each time step, which seldom coincides with the planned position due to disturbances, thus effectively closing the loop.

However, except at the start, it is not necessary to repeat all the steps of Section 4. Since the new position should be close to the planned one, one can apply the linearization scheme of the planning algorithm starting from the last available linearization. The MPC algorithm is summarized next:

Step 1: At time step $k=0$ and starting from x_0 apply the Planning algorithm of Section 4, obtaining a set of PWM inputs Υ_0 that would optimize the planning problem (38) for the next N_p time steps, if there were no disturbances.

Step 2: Apply pulses corresponding to the first time instant; save the rest of them. Set $k=1$.

Step 3: One arrives at x_k, which probably is not the intended value of the state at time k but close. Thus re-planning is necessary.

Step 4: For re-planning, apply the planning algorithm of Section 4. However, to avoid the initial step of having to use a PAM or impulsive model and compute an initial guess, use instead as an initial guess the pulses of Υ_{k-1} that were not used (all of them except for those corresponding to time $k-1$) and guess the remaining pulses (at the end) for instance by using some simple control law. In this work, for the rendezvous example, a terminal law based on the impulsive solution that would cancel the residual velocity at the last step is used. In this way, form an initial guess Υ_k^0.

Step 5: Apply the linearization algorithm of Section 4.4 using Υ_k^0 as initial guess to obtain, after iterating, a new set of pulses Υ_k. Apply the set of pulses corresponding to time k. Save the rest of pulses.

Step 6: Repeat step 3.

6. Example application: spacecraft rendezvous

Rendezvous of spacecraft is the controlled close encounter of two (or more) space vehicles. This work assumes just two vehicles, one of which is the *target vehicle* (which is in a known orbit, and considered passive) and the other is the *chaser spacecraft*, which begins from a known position and maneuvers until it approaches target. As explained in Fehse (2003), only close-range rendezvous is considered, which starts at hundreds of meters and ends when the chaser is very close to target (just several meters, with speeds of centimeters per second).

There are numerous mathematical models for spacecraft rendezvous; which one should be used depends on the parameters of the scenario. In Carter (1998) a survey of numerous mathematical models for spacecraft rendezvous can be found.

For instance, if the target is orbiting in a *circular* Keplerian orbit, the general equations of the relative movement between an active chaser spacecraft close to a passive target vehicle are the linear time-invariant Hill–Clohessy–Wiltshire (HCW) equations (introduced in Hill, 1878; Clohessy & Wiltshire, 1960). While these equations are frequently used in the literature and they are sufficiently accurate for many applications, it must be noted that, in some situations, the HCW equations might not be a good enough approximation—for instance, if the target vehicle is moving in a Keplerian *eccentric* orbit (see Inalhan, Tillerson, & How, 2002) or if some orbital perturbations are taken into account (see for example Humi & Carter, 2008). A more complex model, the Tschauner–Hempel model (see Tschauner & Hempel, 1965; Carter, 1998) assumes that the target vehicle is passive and moving along an elliptical orbit with semi-major axis a and eccentricity e. The system equations are linear time-varying and cannot be exactly integrated in time to obtain a discrete transition model; however, if one substitutes the time t by the *eccentric* anomaly of the target orbit, E, it is possible to obtain explicit expressions for the system evolution in the PWM, impulsive, and PAM actuation cases. This is the model considered in this work.

The rendezvous model can be expressed in cartesian coordinates, but also in the so-called relative orbital elements (see, e.g. Gaias et al., 2014; Sinclair et al., 2014), which are also useful to pose a model predictive control problem for spacecraft applications (see for instance the reference Breger & How, 2005, in which

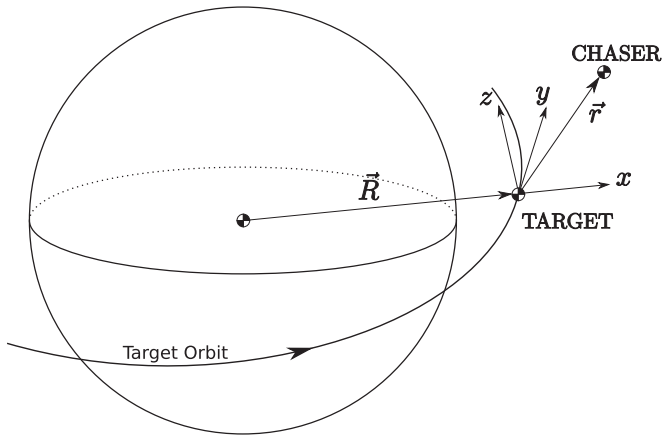

Fig. 2. LVLH frame.

the formation flying maneuver is handled using this technique). For simplicity, the cartesian approach has been chosen in this work.

Let us first establish some notation. Define the orbital mean motion $n = \sqrt{\frac{\mu}{a^3}}$, where μ is the gravitational parameter of the central body around which the target spacecraft is orbiting.

Now, note that t and E are related in a one-to-one fashion by using Kepler's equation

$$n(t - t_p) = E - e\sin E, \tag{63}$$

where t_p is the time at periapsis used as a starting point to measure the eccentric anomaly E. The time t_p is chosen such that it is equal or less than the starting time which is denoted as t_0 (subtracting, if necessary, any number of orbital periods). Kepler's equation is not analytically invertible, but its inverse can be found numerically with any desired degree of precision (see any Orbital Mechanics reference, such as Wie, 1998). Denote its inverse explicitly as a function of time, namely $E = E(t)$. Denote by E_0 the eccentric anomaly corresponding to t_0, this is, $E_0 = E(t_0)$. Then, $E_k = E(t_k) = E(t_0 + kT)$, where T is the sampling time (not to be confused with the orbital period). Call as $r_{x,k}$, $r_{y,k}$, and $r_{z,k}$ the position of the chaser in a local-vertical/local-horizontal (LVLH) frame of reference fixed on the center of gravity of the target vehicle (see Fig. 2) at time t_k. In the (elliptical) LVLH frame, x refers to the radial position, z to the out-of-plane position (in the direction of the orbital angular momentum), and y is perpendicular to these coordinates (not necessarily aligned with the target velocity given that its orbit is not circular). The velocity and inputs of the chaser in the LVLH frame at time t_k are denoted, respectively, by $v_{x,k}$, $v_{y,k}$, and $v_{z,k}$, and by $u_{x,k}$, $u_{y,k}$, and $u_{z,k}$.

If there is no actuation (i.e. $u_{x,k} = u_{y,k} = u_{z,k} = 0$), the resulting evolution equation can be obtained in a simple form (see Yamanaka & Ankersen, 2002). Define first the following matrices Y^E and Y_E^{-1} appearing in Eqs. (64)-(65),where the following symbols are used (expressed in terms of E)

$$Y_E = \begin{bmatrix} s & 0 & 0 & 2/\rho - 3esJ & -c & 0 \\ c(1+1/\rho) & 1/\rho & 0 & -3\rho J & s(1+1/\rho) & 0 \\ 0 & 0 & c/\rho & 0 & 0 & s/\rho \\ \alpha\rho^2 c & 0 & 0 & \alpha(-es - 3e\rho^2 Jc) & \alpha\rho^2 s & 0 \\ \alpha s(-1-\rho^2) & \alpha es & 0 & \alpha\rho(3es\rho J - 3) & \alpha(c + e + c\rho^2) & 0 \\ 0 & 0 & -s\alpha & 0 & 0 & (c+e)\alpha \end{bmatrix}, \tag{64}$$

$$Y_E^{-1} = \frac{3J}{\left(1-e^2\right)} \begin{bmatrix} e\rho^2(1+\rho) & -e^2\rho^2 s & 0 & e^2 s/\alpha & e\rho/\alpha & 0 \\ \rho^2(1+\rho) & -e\rho^2 s & 0 & es/\alpha & \rho/\alpha & 0 \\ 0 & 0 & 0 & 0 & 0 & 0 \\ 0 & 0 & 0 & 0 & 0 & 0 \\ 0 & 0 & 0 & 0 & 0 & 0 \\ 0 & 0 & 0 & 0 & 0 & 0 \end{bmatrix}$$
$$+ \frac{1}{\left(1-e^2\right)} \begin{bmatrix} -s\left(\rho^2 + 2\rho + e^2\right) & es^2(1+\rho) & 0 & \frac{c - 2e/\rho}{\alpha} & -\frac{s(\rho+1)}{\rho\alpha} & 0 \\ -es(1+\rho)^2 & \rho^2(1-ce) + e^2 s^2 & 0 & \frac{ec - 2/\rho}{\alpha} & -\frac{es(\rho+1)}{\rho\alpha} & 0 \\ 0 & 0 & (c+e)\left(1-e^2\right) & 0 & 0 & \frac{-s\left(1-e^2\right)}{\alpha\rho} \\ \rho^2(1+\rho) & -es\rho^2 & 0 & \frac{es}{\alpha} & \frac{\rho}{\alpha} & 0 \\ 3\rho(c+e) - e\rho s^2 & -esc(1+\rho) - e^2 s & 0 & \frac{s}{\alpha} & \frac{c(\rho+1)+e}{\alpha\rho} & 0 \\ 0 & 0 & s\left(1-e^2\right) & 0 & 0 & \frac{c\left(1-e^2\right)}{\alpha\rho} \end{bmatrix} \tag{65}$$

$$\rho = \frac{1-e^2}{1 - e\cos E}, \quad s = \frac{\sqrt{1-e^2}\sin E}{1 - e\cos E}, \quad c = \frac{\cos E - e}{1 - e\cos E}, \tag{66}$$

$$J = \alpha \frac{E - \hat{E} - e(\sin E - \sin \hat{E})}{(1-e^2)^{3/2}}, \quad \alpha = \frac{n}{(1-e^2)^{3/2}}, \tag{67}$$

where $\hat{E}$ in (67) can be substituted by zero or any other desired reference value of E. For instance, if when evaluating (70) one chooses $\hat{E} = E_k = E(t_k)$, then for $Y^{-1}_{E(t_k)}$ one gets $J=0$ and the first matrix in (65) becomes zero.

Then, denoting

$$x_k = \left[r_{x,k} r_{y,k} r_{z,k} v_{x,k} v_{y,k} v_{z,k} \right]^T, \tag{68}$$

the transition matrix is expressed as

$$x_{k+1} = \Phi(t_{k+1}, t_k) x_k, \tag{69}$$

where Φ is obtained from the previously-defined matrices (64) and (65) as

$$\Phi(t_{k+1}, t_k) = Y_{E(t_{k+1})} Y^{-1}_{E(t_k)}. \tag{70}$$

The matrix Y_{t_k} is the fundamental matrix solution of the Tschauner–Hempel model, which is expressed in Yamanaka and Ankersen (2002)[1] as a function of *true* anomaly θ. However there is a one-to-one relation between E and θ given by

$$\tan\frac{\theta}{2} = \sqrt{\frac{1+e}{1-e}} \tan\frac{E}{2}, \tag{71}$$

which is exploited in the sequel.

Using (70), one gets A_k in (16) explicitly, as well as B_k in the impulsive case (explicitly defined in terms of $\Phi(t_{k+1}, t_k)$). To obtain the B_k matrix in the PWM and PAM cases, one needs to solve (8) or (12), respectively, which involves an integral. Defining

$$b_i(r_1, r_2, r_3) = \int_{r_1}^{r_2} \Phi(r_3, s) B_i(s)\, \mathrm{d}s, \tag{72}$$

one has that, from (8),

$$B^W_{k,i}(\tau_{k,i}, \kappa_{k,i}) = b_i(t_k + \tau_{k,i}, t_k + \tau_{k,i} + \kappa_{k,i}, t_{k+1}), \tag{73}$$

and, from (12),

$$B^A_{k,i} = b_i(t_k, t_{k+1}, t_{k+1}). \tag{74}$$

To compute the b_i's, the following integral is needed

$$\int Y^{-1}_{E(t)} C_{i+3}\, \mathrm{d}t, \tag{75}$$

where C_i is a 6-element column vector of zeros with a value of one at row i. For the computation, define the functions $f_i(t)$, for $i = 1, 2, 3$, as the indefinite integrals of (75), in terms of eccentric anomaly

$$f_i(E) = \int Y^{-1}_E C_{i+3} \frac{1 - e\cos E}{n}\, \mathrm{d}E. \tag{76}$$

Once the f_i's are computed, one finds the b_i's as

$$b_i(r_1, r_2, r_3) = Y_{E(r_3)} \left(f_i(E(r_2)) - f_i(E(r_1)) \right) \tag{77}$$

Inserting the expression of (65) in (76) and integrating, one obtains

$$f_1 = \frac{\tilde{e}^{-7/2}}{2\alpha^2} \begin{bmatrix} 2(1+6e^2)S - 3e(2+e^2)E + e^2 Ch + e^3 \hat{S}/2 \\ 2e(8-e^2)S - (4+7e^2-2e^4)E + eCh + e^2\hat{S}/2 \\ 0 \\ -2eC(1-e^2)^{3/2} \\ -2C(1-e^2)^{3/2} \\ 0 \end{bmatrix}, \tag{78}$$

$$f_2 = \frac{\tilde{e}^{-3}}{2\alpha^2} \begin{bmatrix} C(4(1+e^2) - eC) - eEh - 3eE^2 \\ eC(10 - 2e^2 - eC) - Eh - 3E^2 \\ 0 \\ 2E(1-e^2)^{3/2} \\ \sqrt{1-e^2}\left(4S - e\left(3E + \hat{S}/2\right)\right) \\ 0 \end{bmatrix}, \tag{79}$$

$$f_3 = \frac{\tilde{e}^{-5/2}}{4\alpha^2} \begin{bmatrix} 0 \\ 0 \\ 2\sqrt{1-e^2}C(2-eC) \\ 0 \\ 0 \\ 4(e^2+1)S - e\left(6E + \hat{S}\right) \end{bmatrix}, \tag{80}$$

where $\tilde{e} = 1-e^2$, $S = \sin(E)$, $\hat{S} = \sin(2E)$, $C = \cos E$, $h = 6\alpha(\hat{E} - E - e\sin(\hat{E}))$. Similar expressions for the B matrices can be found in Ankersen (2010), however using a slightly different definition of reference axes.

Note that, using these formulas, it is possible to express (16) explicitly for all actuation types. This greatly speeds up the algorithms.

6.1. Constraints for the rendezvous problem

Besides the input constraints (which were given in Section 3.1.2), the inequality state constraints which were generically specified in Section 3.1.1 are, in general, related to safety and sensing considerations (see e.g. Breger & How, 2008). In this work, it is considered that during rendezvous the chaser vehicle has to remain inside a line of sight (LOS) area. To simplify the constraint,[2] in this work a 2-D LOS area is used as shown in Fig. 3. This LOS region is the intersection of a cone, given by the equations $r_y \geq c_{LOS}(r_x - r_{x_0})$ and $r_y \geq -c_{LOS}(r_x + r_{x_0})$, and the region $r_y \geq 0$.

The LOS constraint is $C_{LOS} x_k \leq d_{LOS}$, where

$$C_{LOS} = \begin{bmatrix} 0 & -1 & 0 & 0 & 0 & 0 \\ c_{LOS} & -1 & 0 & 0 & 0 & 0 \\ -c_{LOS} & -1 & 0 & 0 & 0 & 0 \end{bmatrix},$$
$$d_{LOS} = \begin{bmatrix} 0 \\ c_{LOS} r_{x_0} \\ c_{LOS} r_{x_0} \end{bmatrix}. \tag{81}$$

Using the compact formulation that was developed in Section

[1] These expressions slightly differ from Yamanaka and Ankersen (2002) because the two transformation matrices that appear in that paper have been pre-multiplied; also, the reference axes are not the same.

[2] More complicated constraints could be considered, see Gavilan et al. (2012) for examples including a rotating LOS constraint.

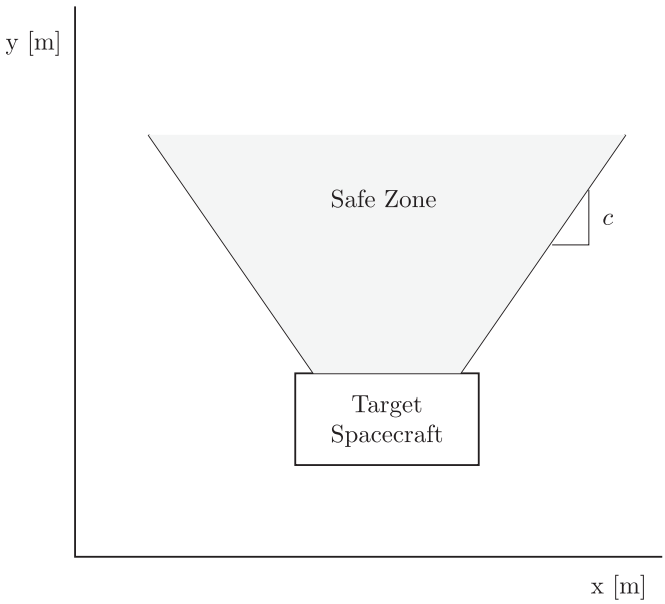

Fig. 3. Line of sight region.

2, the constraints equations for the state can be rewritten as:

$$C_S \mathcal{X} \leq d_S, \tag{82}$$

where C_S and d_S are given by:

$$C_S = \begin{bmatrix} C_{LOS} & & \\ & \ddots & \\ & & C_{LOS} \end{bmatrix}, \quad d_S = \begin{bmatrix} d_{LOS} \\ \vdots \\ d_{LOS} \end{bmatrix}. \tag{83}$$

Notice that the subscript k is no longer needed in C_S and d_S, since the state constraints do not vary along the prediction horizon.

Then, using Eq. (20), one can reformulate the LOS constraints as constraints for the control signals, starting at time step t_k, in the following way:

$$C_S G_k \mathcal{U}_k \leq d_S - C_S F_k x_0. \tag{84}$$

7. Simulation results

For simulations the following values have been used: N_p=50 as planning horizon, T=60 s, and $\bar{u} = 10^{-1}$ N/kg. The target orbit has e=0.7 and perigee altitude $h_p = 500$ km. Initial conditions were $\theta_0 = 45°$, $\mathbf{r}_0 = [0.25\ 0.4\ \ -0.2]^T$ km, $\mathbf{v}_0 = [0.005\ \ -0.005\ \ -0.005]^T$ km/s. The LOS constraint is defined by $x_0 = 0.001$ km and $c_{LOS} = \tan 30°$. For the cost function, α has been set to 10^3 and Q_k as

$$Q_k = \begin{bmatrix} R_{k+1} & & \\ & \ddots & \\ & & R_{k+N_p} \end{bmatrix}, \tag{85}$$

where R_k is defined as

$$R_k = h(k - k_a)\mathrm{I}_{6\times 6} \tag{86}$$

where, h is the step function and k_a is the desired arrival time for rendezvous. Notice that the dimensions of each block matrix are shown for disambiguation. The reason for choosing (86) is that it is desired to arrive at the origin at time k_a (and *remain* there) and at the same time minimize the control effort. In the sequel k_a=N_p, so the spacecraft is expected to rendezvous after about 50 min.

In the simulations three algorithms were considered: first, an impulsive open-loop trajectory planner, as described in Section 4.1. Next, closed-loop simulations using MPC but considering impulsive instead of PWM actuation in the model (this algorithm is denoted as impulsive MPC). Finally, closed-loop simulations using MPC, based on the PWM algorithms as explained in Section 5, with initial solutions computed using the impulsive hot-start (the PAM hot-start produces similar solutions with slightly worse cost). All algorithms are simulated on the more realistic model with PWM actuation. Since the first and second methods use the impulsive models but are simulated with PWM actuation, the impulsive signals are subsequently transformed to PWM inputs using the algorithm of Section 4.2.

Compare first the algorithms without disturbances. The trajectories (projected on the target orbital plane) are shown in Fig. 4. The open-loop impulsive solution does not achieve rendezvous and drifts away, which is to be expected given that the planning model and the simulation model are not the same, whereas the other solutions successfully reach the origin. At the predefined rendezvous time (50 min), the chaser vehicle is about 5 m away from the target. Taking advantage of the receding-horizon formulation, the algorithm can be left running for longer and then chaser vehicle keeps asymptotically approaching the target, in particular after two more minutes, the chaser is at less than half a meter from the target, which is sufficiently close to start the next phase of rendezvous (docking or berthing). On the other hand, it is remarkable that the impulsive MPC is able to mostly compensate its imperfect thruster model and reached the target in 50 min, however it must be taken into account that for very small impulses both models do not disagree by much, so it is mainly at the beginning, when more strong actuation is necessary, that both algorithms differ. The PWM-MPC algorithm had a cost of 15.2 m/s and the impulsive MPC had a cost of 16 m/s. Thus, while a basic (impulsive) MPC is able to rendezvous, the use of an imperfect model has some fuel costs. In addition, the impulsive MPC does not satisfy the line-of-sight constraints for a period of time. It is interesting to compare the resulting pulses of both algorithms, whose duration is represented in Fig. 5. It can be seen that both algorithms start with a strong pulse in the y direction to compensate for the initial velocity; soon, the impulsive MPC uses many corrections of small magnitude whereas the PWM-MPC algorithm only has a few of them. This justifies its smaller cost.

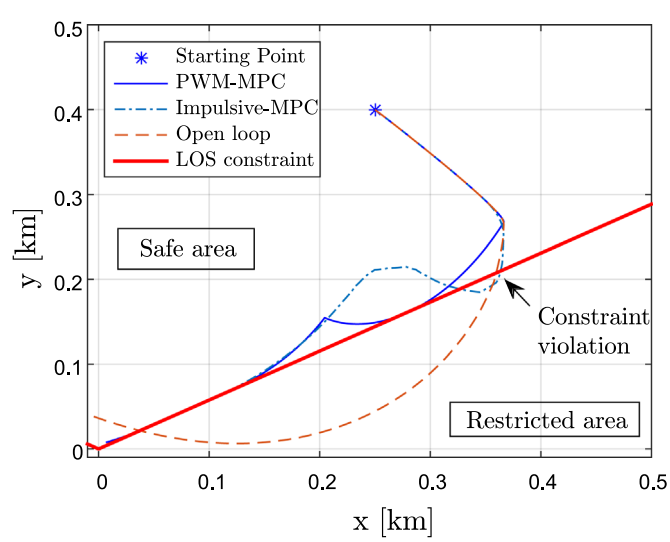

Fig. 4. System trajectories in the target orbital plane: open-loop PWM inputs computed from impulsive solution (dashed), closed-loop Model Predictive Control with PWM inputs using impulsive model (dot-dashed), and closed-loop Model Predictive Control with PWM inputs using the PWM planning algorithm (solid).

Please cite this article as: Vazquez, R., et al. (2016), http://dx.doi.org/10.1016/j.conengprac.2016.06.017

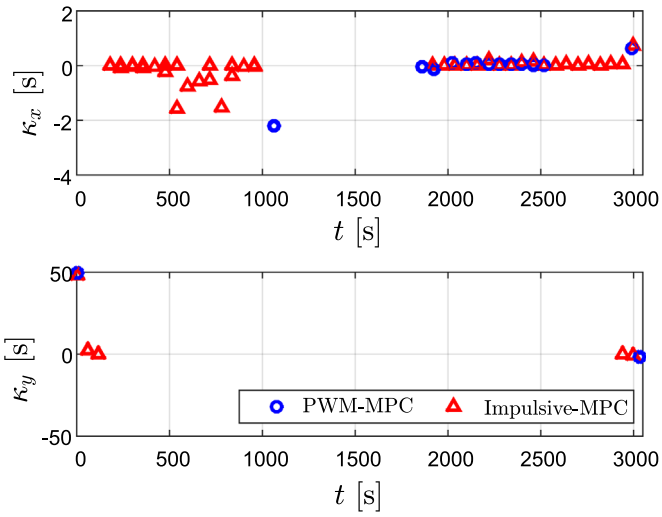

Fig. 5. Duration of pulses in the target orbital plane (x and y directions): closed-loop Model Predictive Control with PWM inputs using impulsive model (triangles), and closed-loop Model Predictive Control with PWM inputs using the PWM planning algorithm (circles). Pulses lasting less than 2 ms have not been represented. Negative values correspond to negative pulses.

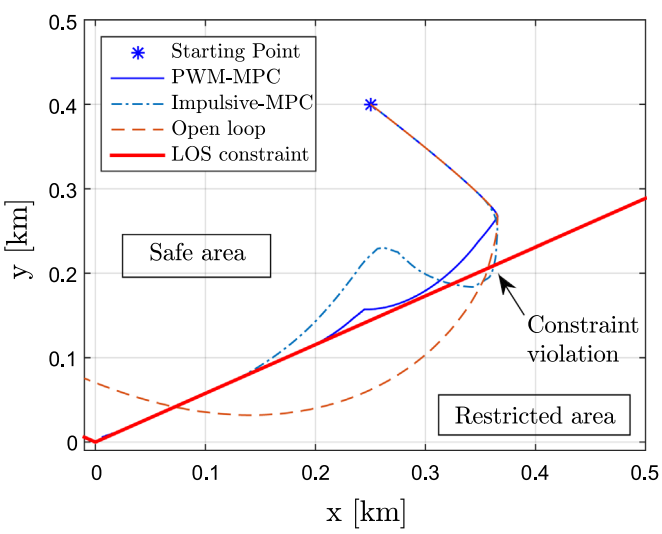

Fig. 6. System trajectories in the target orbital plane, with inexact orbit model: open-loop PWM inputs computed with the planning algorithm (dashed), closed-loop Model Predictive Control with PWM inputs using impulsive model (dot-dashed), and closed-loop Model Predictive Control with PWM inputs using the PWM planning algorithm (solid).

Next, Fig. 6 shows a simulation where the real orbit is different from the reference orbit used in the model (the real eccentricity is $e=0.83$, the real perigee altitude is $h_p = 525$ km, and the real $\theta_0 = 60°$). Both MPC algorithms asymptotically approach the origin (as in the previous scenario, the chaser vehicle approaches the target to less than 0.5 m in 52 min). The impulsive MPC again exits the line-of-sight region. In this case both algorithms had imperfect models and the costs were similar, in particular the cost for the PWM MPC algorithm was 15.3 m/s, whereas the impulsive MPC had the same cost of 16 m/s as in the perfectly-known orbit case. The simulations were performed by using MATLAB and the *Gurobi* optimization package (see Gurobi Optimization, Inc., 2014), which uses a barrier (interior point) method, even though other methods that provide more guarantees in the optimization process could be implemented, see e.g. Guiggiani, Kolmanovsky, Patrinos, and Bemporad (2015). In each step of the PWM algorithm, the optimizer has to solve a quadratic programming problem with 600 decision variables and 150 constraints, and Gurobi took between 16 and 26 iterations. A maximum number of 6 steps were sufficient to achieve convergence in the case under study.

It must be noted that, while the PWM MPC verifies the line-of-sight constraints in the two considered cases, the proposed method (based on linearization) does not offer any guarantees that this will be the case. A possible idea to enforce constraint satisfaction would be including an estimate of linearization error in the model. Taylor's theorem offers such a bound based on the second derivative of the actuation term with respect to PWM variables. This term can be computed analytically in the same fashion that the first-order derivatives were computed. Such a bound could be used to robustify the constraints with respect to the linearization error. However, since the bound would contain the maximum possible linearization error, the resulting constraints might be too conservative and even lead to an unfeasible optimization problem. Thus, further research is necessary to confirm the validity of this idea, which will be explored in future works.

8. Concluding remarks

This paper has presented a MPC algorithm that computes optimal PWM inputs for LTV systems. The algorithm is based on an initial approximation with either PAM or impulsive inputs, followed by iterative explicit linearization. As an application, the problem of rendezvous in elliptical orbits has been considered. In particular, the algorithm might be particularly useful for satellites with small specific thrust. The algorithm improves the fuel cost of an impulsive-only MPC (with the impulses posteriorly transformed to PWM inputs), and is able to satisfy safety constraints and handle disturbances such as imperfect knowledge of the target's orbit. This algorithm would help avoiding having to include a PWM approximation term in the "uncertainty budget" and therefore save costs. However, inclusion of real-life constraints, a computational study including real spacecraft hardware, and more realistic simulations are needed to validate the method.

Possible future lines of research include the following. First, it will be of great interest to study the convergence of the planning algorithm (by analyzing other SQP schemes, possibly under additional, more restrictive assumptions). Another possible line would be guaranteeing constraint satisfaction as explained at the end of Section 7. Another option would be to guarantee recursive feasibility of the MPC optimization problem, by converting hard constraints into soft ones by using, e.g. a distance-from-set function. Finally, the formulation of the cost function in the solution means the control is attractive, but more analysis is necessary to prove stability of the closed-loop system, which should be feasible by using previous MPC results (see for instance Grune & Pannek, 2011; Goodwin, Seron, & De Dona, 2005). Addressing this issue would also help to analyze the convergence of the method.

Acknowledgments

The authors acknowledge financial support from the Spanish Ministerio de Economía y Competitividad under grants DPI2008–05818 and MTM2015-65608-P.

References

Ankersen, F. (2010). *Guidance, navigation, control and relative dynamics for spacecraft proximity maneuvers* (Ph.D. thesis).

Arzelier, D., Kara-Zaitri, M., Louembet, C., & Delibasi, A. (2011). Using polynomial

optimization to solve the fuel-optimal linear impulsive rendezvous problem. *Journal of Guidance, Control, and Dynamics*, *34*, 1567–1572.

Arzelier, D., Louembet, C., Rondepierre, A., & Kara-Zaitri, M. (2013). A new mixed iterative algorithm to solve the fuel-optimal linear impulsive rendezvous problem. *Journal of Optimization Theory and Applications*, *159*, 210–230.

Asawa, S., Nagashio, T., & Kida, T. (2006). Formation flight of spacecraft in earth orbit via MPC. In *SICE-ICASE international join conference*.

Bernelli-Zazzera, F., Mantegazza, P., & Nurzia, V. (1998). Multi-pulse-width modulated control of linear systems. *Journal of Guidance, Control, and Dynamics*, *21*(1), 64–70.

Breger, L., & How, J. (2005). J2-modified gve-based mpc for formation flying spacecraft. In *Collection of technical papers—AIAA guidance, navigation, and control conference* (Vol. 1, pp. 158–169).

Breger, L., & How, J. P. (2008). Safe trajectories for autonomous rendezvous of spacecraft. *Journal of Guidance, Control, and Dynamics*, *31*(5), 1478–1489.

Camacho, E., & Bordons, C. (2004). *Model predictive control* (2nd edition). London: Springer-Verlag.

Carter, T. E. (1998). State transition matrices for terminal rendezvous studies: *Brief survey and new example. Journal of Guidance, Control, and Dynamics*, *21*(1), 148–155.

Clohessy, W. H., & Wiltshire, R. S. (1960). Terminal guidance systems for satellite rendezvous. *Journal of Aerospace Science*, *27*(9), 653–658.

D'Amico, S., Ardaens, J.-S., Gaias, G., Benninghoff, H., Schlepp, B., & Jörgensen, J. L. (2013). Noncooperative rendezvous using angles-only optical navigation: *System design and flight results. Journal of Guidance, Control, and Dynamics*, *36*(6), 1576–1595.

Deaconu, G., Louembet, C., & Théron, A. (2014). Minimizing the effects of the navigation uncertainties on the spacecraft rendezvous precision. *Journal of Guidance, Control, and Dynamics*, *37*(2), 695–700.

Deaconu, G., Louembet, C., & Théron, A. (2015). Designing continuously constrained spacecraft relative trajectories for proximity operations. *Journal of Guidance, Control, and Dynamics*, *38*(7), 1208–1217.

Fehse, W. (2003). *Automated rendezvous and docking of spacecraft*. Cambridge, UK: Cambridge University Press.

Gaias, G., D'Amico, S., & Ardaens, J.-S. (2014). Angles-only navigation to a noncooperative satellite using relative orbital elements. *Journal of Guidance, Control, and Dynamics*, *37*(2), 439–451.

Gavilan, F., Vazquez, R., & Camacho, E. F. (2009). Robust model predictive control for spacecraft rendezvous with online prediction of disturbance bound. In *Proceedings of AGNFCS'09*, Samara, Russia.

Gavilan, F., Vazquez, R., & Camacho, E. F. (2012). Chance-constrained model predictive control for spacecraft rendezvous with disturbance estimation. *Control Engineering Practice*, *20*(2), 111–122.

Goodwin, G., Seron, M. M., & De Dona, J. (2005). *Constrained control and estimation: An optimisation approach*. London: Springer-Verlag.

Grune, L., & Pannek, J. (2011). *Nonlinear model predictive control: Theory and algorithms*. London: Springer-Verlag.

Guiggiani, A., Kolmanovsky, I., Patrinos, P., & Bemporad, A. (2015). Fixed-point constrained model predictive control of spacecraft attitude. In *Proceedings of 2015 American control conference* (pp. 2317–2322).

Gurobi Optimization, Inc. (2014). Gurobi optimizer reference manual. URL ⟨http://www.gurobi.com⟩.

Hartley, E. N., Trodden, P. A., Richards, A. G., & Maciejowski, J. M. (2012). Model predictive control system design and implementation for spacecraft rendezvous. *Control Engineering Practice*, *20*(7), 695–713.

Hill, G. (1878). Researches in lunar theory. *American Journal of Mathematics*, *1*(3), 5–26 129–147, 245–260.

Houska, B., Ferreau, H., & Diehl, M. (2011). ACADO toolkit–An open-source framework for automatic control and dynamic optimization. *Optimal Control Applications and Methods*, *32*(3), 298–312.

Humi, M., & Carter, T. (2008). Orbits and relative motion in the gravitational field of an oblate body. *Journal of Guidance, Control, and Dynamics*, *31*(3), 522–532.

Ieko, T., Ochi, Y., & Kanai, K. (1999). New design method for pulse-width modulation control systems via digital redesign. *Journal of Guidance, Control, and Dynamics*, *22*(1), 123–128.

Inalhan, G., Tillerson, M., & How, J. P. (2002). Relative dynamics and control of spacecraft formations in eccentric orbits. *Journal of Guidance, Control, and Dynamics*, *25*(1), 48–59.

Jewison, C., Erwin, R. S., & Saenz-Otero, A. (2015). Model predictive control with ellipsoid obstacle constraints for spacecraft rendezvous. In *ACNAAV 2015 IFAC workshop*.

Kim, H. J., Shim, D. H., & Sastry, S. (2002). Nonlinear model predictive tracking control for rotorcraft-based unmanned aerial vehicles. In *Proceedings of ACC* 2002.

Larsson, R., Berge, S., Bodin, P., & Jönsson, U. (2006). Fuel efficient relative orbit control strategies for formation flying and rendezvous within prisma. In *Proceedings of the 29th AAS guidance and control conference*.

Leomanni, M., Rogers, E., & Gabriel, S. B. (2014). Explicit model predictive control approach for low-thrust spacecraft proximity operations. *Journal of Guidance, Control, and Dynamics*, *37*(6), 1780–1790.

Louembet, C., Arzelier, A., & Deaconu, G. (2015). Robust rendezvous planning under maneuvering errors. *Journal of Guidance, Control, and Dynamics*, *38*(1), 76–93.

Nocedal, J., & Wright, S. (2006). *Numerical optimization* (2nd edition). New York: Springer.

Richards, A. G. & How, J. (2003). Performance evaluation of rendezvous using model predictive control. *AIAA paper* 2003-5507.

Rossi, M. & Lovera, M. (2002). A multirate predictive approach to orbit control of small spacecraft. In *Proceedings of ACC 2002*.

Rugh, W. J. (1996). *Linear system theory* (2nd edition). Upper Saddle River, NJ, USA: Prentice-Hall, Inc.

Shieh, L.-S., Wang, W.-M., & Sunkel, J. (1996). Design of PAM and PWM controllers for sampled-data interval systems. *Journal of Dynamic Systems, Measurement, and Control*, *118*(4), 673–681.

Sinclair, A. J., Sherrill, R. E., & Lovell, T. A. (2014). Calibration of linearized solutions for satellite relative motion. *Journal of Guidance, Control, and Dynamics*, *37*(4), 1362–1367.

Tschauner, J., & Hempel, P. (1965). Rendevous zu einem in elliptischer bahn umlaufenden. *Ziel Acta Astronaut II*, *2*, 104–109.

Vazquez, R., Gavilan, F., & Camacho, E. F. (2011). Trajectory planning for spacecraft rendezvous with on/off thrusters. In 2011 *Proceedings of IFAC world congress*.

Vazquez, R., Gavilan, F., & Camacho, E. F. (2014). Trajectory planning for spacecraft rendezvous in elliptical orbits with on/off thrusters. In *IFAC world congress*, Cape Town.

Vazquez, R., Gavilan, F., & Camacho, E. F. (2015). Model predictive control for spacecraft rendezvous in elliptical orbits with on/off thrusters. In *ACNAAV 2015 IFAC workshop*.

Weiss, A., Kolmanovsky, I., Baldwin, M., & Erwin, R. S. (2012). Model predictive control of three dimensional spacecraft relative motion. In 2012 *American Control Conference* (*ACC*). IEEE, pp. 173–178.

Wie, B. (1998). Space vehicle dynamics and control. AIAA, AIAA Education Series, Reston, VA.

Yamanaka, K., & Ankersen, F. (2002). New state transition matrix for relative motion on an arbitrary elliptical orbit. *Journal of Guidance, Control, and Dynamics*, *25*(1), 60–66.

Please cite this article as: Vazquez, R., et al. (2016), http://dx.doi.org/10.1016/j.conengprac.2016.06.017